Crystal orientation effects on wurtzite quantum well electromechanical fields

Lars Duggen* and Morten Willatzen
Mads Clausen Institute, University of Southern Denmark, Alsion 2, DK-6400 Sønderborg, Denmark
(Received 4 January 2010; revised manuscript received 12 October 2010; published 4 November 2010)

A one-dimensional continuum model for calculating strain and electric field in wurtzite semiconductor heterostructures with arbitrary crystal orientation is presented and applied to GaN/AlGaN and ZnO/MgZnO heterostructure combinations. The model is self-consistent involving feedback couplings of spontaneous polarization, strain, and electric field. Significant differences between fully coupled and semicoupled models are found for the longitudinal and shear-strain components as a function of the crystal-growth direction. In particular, we find that the semicoupled model, typically used in the literature for semiconductors, is inaccurate for ZnO/MgZnO heterostructures where shear-strain components play an important role. An interesting observation is that a growth direction apart from $[\bar{1}2\bar{1}0]$ exists for which the electric field in the quantum well region becomes zero. This is important for, e.g., optimization of light-emitting-diode quantum efficiency.

DOI: 10.1103/PhysRevB.82.205303 PACS number(s): 77.65.Ly

I. INTRODUCTION

In recent years, quantum semiconductor structures consisting of group-III nitrides such as wurtzite AlN/GaN have received much attention due to their applications in optoelectronic devices, such as GaN light-emitting diode (LED) (Ref. 1) and laser diodes in the blue and UV regions,[2–4] and for Heterostructure Field Effect Transistor (HFET) applications.[5] Besides the nitride-based devices, also group-II oxides have be examined considerably for both highly efficient laser diodes[6–10] as well as high performance field effect transistors.[11,12] It has been shown that the induced piezoelectric field plays a significant role for both band structure and optical gain.[13] However, the orientation of the crystal structure significantly modifies the electronic band structure through strain effects.[14] It has been shown experimentally for open-circuit conditions that growth along crystal directions other than the [0001] direction leads to an increase in the quantum efficiency by decreasing the strain-induced electric field in the quantum well region, possibly leading the way to highly efficient white LEDs.[15] There have been several theoretical works studying the effect of crystal orientation on the piezoelectric field in strained wurtzite quantum wells and antiwell structures (both for GaN and ZnO compounds),[14,16–20] mostly finding the strain by minimizing elastic energy (semicoupled model) and calculating the piezoelectric polarization from this. However, the piezoelectric effect consists not only of a strain-induced polarization,[21,22] it also includes feedback couplings of the electric field and polarization on the strain to be accounted for when minimizing the total free energy.[22,23] Furthermore, it has been shown for wurtzite AlGaN compounds grown along the [0001] direction as well as for zinc blende InGaN at specific crystal orientations that this effect changes the magnitude of the strain significantly[23,24] thus stipulating that a fully coupled model is important when investigating crystal orientation effects.

In this work, we use a one-dimensional model to calculate the strain and electric fields in wurtzite $GaN/Al_xGa_{1-x}N$ and $ZnO/Mg_xZn_{1-x}O$ heterostructures with arbitrary growth direction taking into full account piezoelectric and lattice mismatch contributions. In general, this is done by solving the Schrödinger equation along with Maxwell-Poisson equation and Newton's second law. In the present work, we simplify the analysis by disregarding free-charge carriers. This allows us to analytically solve the coupled equations of Newton's second law and Maxwell-Poisson only. In addition, we consider the electric potential to be applied homogeneously by electrodes spanning the entire cross section, such that electric field components transverse to the growth direction vanish.

II. THEORY

In the static case, Newton's second law for a solid and the Maxwell-Poisson equation in the absence of free-charge carriers supplemented by the fully coupled constitutive equations in electromechanical fields read[24]

$$\nabla \cdot \mathbf{T} = 0, \tag{1}$$

$$\nabla \cdot \mathbf{D} = 0, \tag{2}$$

$$\mathbf{T} = -\mathbf{e}^T \cdot \mathbf{E} + \mathbf{c}^{\mathbf{E}} \cdot \mathbf{S}, \tag{3}$$

$$\mathbf{D} = \boldsymbol{\epsilon}^{\mathbf{S}} \cdot \mathbf{E} + \mathbf{P} + \mathbf{e} \cdot \mathbf{S}, \tag{4}$$

where **T**, **E**, **S**, **D**, and **P** are the stress tensor, electric field, strain tensor, electric displacement, and spontaneous polarization, respectively. The coefficients **e**, $\mathbf{c}^{\mathbf{E}}$, and $\boldsymbol{\epsilon}^{\mathbf{S}}$ are the piezoelectric **e** tensor, stiffness tensor at constant electric field, and permittivity at constant strain, respectively. As we use the Voigt notation, the superscript T denotes the matrix transpose. The semicoupled model corresponds to setting $-\mathbf{e}^T=0$ in Eq. (3).

In the following, a one-dimensional model in z is considered (imposing $\frac{\partial}{\partial x}=\frac{\partial}{\partial y}=0$). In order to model effects due to differences in heterostructure growth and unit-cell c-axis directions, the coordinate system is transformed using two subsequent rotations as shown in Fig. 1.

The combined rotation leads to the following transformation of the position vector:

$$\widehat{\mathbf{x}'} = \widehat{\mathbf{x}_\phi} = \hat{\mathbf{x}} \cos(\phi) + \hat{\mathbf{y}} \sin(\phi), \tag{5}$$

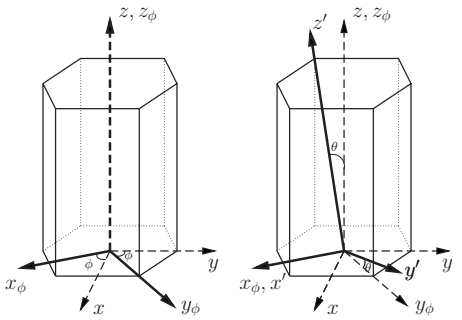

FIG. 1. (a) First rotation of angle ϕ around the z axis. (b) Second rotation of angle θ around the intermediate x_ϕ axis. The growth direction of the heterostructure is always chosen to be along the z' direction such that the interface planes are coplanar with the $x'y'$ plane.

$$\widehat{\mathbf{y}'} = \widehat{\mathbf{y}}_\phi \cos(\theta) + \widehat{\mathbf{z}}_\phi \sin(\theta) = -\hat{\mathbf{x}} \sin(\phi)\cos(\theta) + \hat{\mathbf{y}} \cos(\phi)\cos(\theta) + \hat{\mathbf{z}} \sin(\theta), \tag{6}$$

$$\widehat{\mathbf{z}'} = -\widehat{\mathbf{y}}_\phi \sin(\theta) + \widehat{\mathbf{z}}_\phi \cos(\theta) = \hat{\mathbf{x}} \sin(\phi)\sin(\theta) - \hat{\mathbf{y}} \cos(\phi)\sin(\theta) + \hat{\mathbf{z}} \cos(\theta). \tag{7}$$

A similar rotation of electromechanical fields, material parameters, and differential operators following Refs. 22 and 24 allows us to recast Eqs. (3) and (4) in rotated coordinates. Note that all growth directions can be modeled since $\widehat{\mathbf{z}'}$ traces a sphere with center (0,0,0) over the angular parameter ranges $0 \le \phi \le 2\pi$ and $0 \le \theta \le \pi$. Since there is no lattice mismatch or spontaneous polarization contribution to the $S_5 = 2S_{x'z'}$ and $S_6 = 2S_{x'y'}$ strain components when the growth direction coincides with the c axis of the wurtzite lattice and since any rotation of the growth direction only leads to mixing of the S_5 and S_6 components the latter components are independent of the growth direction. In addition, the S_i components $(i=1,2,3,4)$ are coupled only for a general rotation of the growth direction; this explains why $S_4 = 2S_{y'z'}$ changes with growth direction, refer to Fig. 6. As a corollary, we note that all transformed parameter matrices are independent of ϕ (cylindrical symmetry) when the growth axis is along the c axis.[16,25,26]

Henceforth, we leave out primes on rotated coordinates as this should not cause confusion. In a one-dimensional model, Eq. (2) requires D_z to be a constant in each layer such that continuity of D_z implies that $D_z = D$ is constant throughout the structure. From the static Maxwell's equation $\nabla \times \mathbf{E} = (-\frac{\partial E_y}{\partial z}, \frac{\partial E_x}{\partial z}, 0) = 0$, where the first equality applies in the present one-dimensional model assumption, E_x, E_y are constants in each layer and continuity now forces E_x and E_y to be constant throughout the structure. We choose $E_x = E_y = 0$ at both outer boundaries, assuming that a voltage is applied over metal electrodes spanning the end surfaces. To enforce $E_x = E_y = 0$ through the whole structure, Eq. (4) is used to write

$$[\boldsymbol{\epsilon}^{(i)-1}\mathbf{D}^{(i)}]_1 = [\boldsymbol{\epsilon}^{(i)-1}\mathbf{P}^{(i)}]_1 + [\boldsymbol{\epsilon}^{(i)-1}\mathbf{e}^{(i)}\mathbf{S}^{(i)}]_1, \tag{8}$$

$$[\boldsymbol{\epsilon}^{(i)-1}\mathbf{D}^{(i)}]_2 = [\boldsymbol{\epsilon}^{(i)-1}\mathbf{P}^{(i)}]_2 + [\boldsymbol{\epsilon}^{(i)-1}\mathbf{e}^{(i)}\mathbf{S}^{(i)}]_2, \tag{9}$$

where $i=1,2,3$ indicates the respective material layer, such that these equations apply in each material layer separately. As usual, the subscripts 1 and 2 represent x and y, respectively. Use of Eqs. (3), (4), (8), and (9) and the above interface boundary conditions allows us to find the strain, the electric displacement field components $D_x^{(i)}, D_y^{(i)}$, and the electric field component $E_z^{(i)}$ using Eq. (4). Note that, from Eqs. (1), (3), and (4) and the fact that $\mathbf{D}$ and $\mathbf{P}$ are divergenceless in one dimension in each layer, we find that $\nabla \cdot \mathbf{S} = 0$, i.e., the strain is constant in each layer.

In order to obtain an idea about the difference between the semicoupled and fully coupled models, the analytical closed form solutions corresponding to the direction [0001] have already been found to be[23]

$$a_{mis} = \frac{a^{(2)} - a^{(1)}}{a^{(1)}}, \tag{10}$$

$$S_{xx} = S_{yy} = -a_{mis}, \tag{11}$$

$$S_{zz}^{(1)} = S_{zz}^{(3)} = e_{z3}^{(1)} \frac{D - P_z^{(1)}}{e_{z3}^{(1)^2} + c_{33}^{(1)} \epsilon_{zz}^{(1)}}, \tag{12}$$

$$S_{zz}^{(2)} = \frac{e_{z3}^{(2)}(D - P_z^{(2)}) + 2a_{mis}(e_{z1}^{(2)} e_{z3}^{(2)} + c_{13}^{(2)} \epsilon_{zz}^{(2)})}{e_{z3}^{(2)^2} + c_{33}^{(2)} \epsilon_{zz}^{(2)}}, \tag{13}$$

where superscript (i) indicates the layer [$i=2$ for the middle layer and $i=1$ $(i=3)$ for the left (right) layer]. Note that in the semicoupled model, the expression for $S_{zz}^{(2)}$ becomes $2a_{mis}\frac{c_{13}^{(2)}}{c_{33}^{(2)}}$, i.e., the well-known Poisson ratio expression is obtained.

We emphasize that the preceding continuum modeling strain discussions with boundary conditions automatically allow for relaxation of the lattice constant along the z' direction for the whole heterostructure including cladding layers. This is a simplified standard model in which the middle layer is fully accommodated to the constrained upper and lower layers. The analysis carried out in this work assumes that misfit dislocations and other imperfections are not present in the overall structure which is a good approximation, in particular, for small middle-layer thicknesses. We emphasize, however, that misfit dislocations can be present in cases with larger middle-layer thicknesses.[5] The maximum middle layer thickness d_c for pseudomorphic growth depends on the strain in the middle layer itself and can be estimated by[27]

$$d_c \approx \frac{a^{(1)}}{2\left|\frac{a^{(2)} - a^{(1)}}{a^{(2)}}\right|}. \tag{14}$$

In the present case, d_c is about 10 nm. Above the critical thickness, imperfections are found in the middle layer. Evidently, the choice of boundary conditions affects the electromechanical field distributions. A comparison of Keating valence force field (VFF) atomistic strain results[28] and continuum strain results shows good agreement when equivalent boundary conditions are employed for the comparison, i.e.,

when free boundaries are assumed (stress-free boundary conditions) in the continuum model while external coupling of surface atoms to "vacuum atoms" is assumed in the VFF model.[29]

Electrostriction and nonlinear permittivity

It is relevant to recall the influence of nonlinear electromechanical effects in nanostructures. Experimental results by Guy *et al.*[30] indicate giant electrostriction coefficients in wurtzite GaN being two orders of magnitude larger than corresponding values reported experimentally for wurtzite AlN and MgO![31] Stimulated by the work of Guy *et al.*, one of us (M.W.) initiated a study of electrostriction in wurtzite materials and influence on electromechanical fields with emphasis to GaN/AlN heterostructures.[32] Using the experimental electrostriction value of Ref. 30 it was shown that electrostriction effects have a strong impact on, e.g., GaN/AlN strain distributions and the speed of sound. Since that study we have carried out independent GaN *ab initio* calculations of electrostriction coefficients in the framework of ABINIT.[33] The computed electrostriction coefficients obtained using ABINIT are comparable to experimental results on similar wurtzite structures (AlN, MgO) (Ref. 31) but in conflict with the experimental result of Guy *et al.* in the case of wurtzite GaN. While there is still much uncertainty in the literature regarding electrostriction coefficients, the above result led us to believe that the experimental data in Ref. 30 were either in error or due to some extrinsic effect. These latter findings indeed indicate a minor role of electrostriction in wurtzite heterostructures and explain why we have disregarded electrostriction effects in the present work.

In a previous paper,[34] it was shown that nonlinear permittivity effects become important at electric field values near and above 10^9 V/m, and that such high electric field values exist in AlN/GaN heterostructures in the absence of interface charges. According to Ref. 28, the inclusion of nonlinear permittivity effects can lead to approximately 20% difference in electric field values. In turn, this difference leads to approximately 20% variations in the difference between fully coupled and semicoupled strain results (note that semicoupled model strain results are independent of the electric field and only dependent on the lattice mismatch). With these considerations in mind, a similar variation of approximately 20% is expected in electric fields and differences between fully coupled and semicoupled strain values in the absence of interface charges as considered in the present work but it should be noted that the presence of interface charges diminishes the influence of nonlinear permittivity effects.[34]

III. RESULTS

A. GaN/$Ga_{1-x}Al_xN$/GaN antiwell

For a varying angle θ using the fully and semicoupled models and the parameters given in Table I, the results in Figs. 2 and 3 are obtained for a GaN/$Ga_{1-x}Al_xN$/GaN antiwell structure also considered in Refs. 5 and 16. Note that S_{xz} is always zero as explained in Sec. II. Graphs for the shear strain S_{yz} have been left out because this strain component is significantly smaller than the longitudinal strain for all growth directions. Further, the angle θ can be linked to Miller-index notation by taking directions $[\bar{1}2\bar{1}N]$ with $N=2c/[a\tan(\theta)]$. Hence, $\theta=0$ corresponds to [0001], $\theta\approx 38.7°$ to $[\bar{1}2\bar{1}4]$, $\theta\approx 46.9°$ to $[\bar{1}2\bar{1}3]$, and $\theta\approx 58°$ to $[\bar{1}2\bar{1}2]$, being a cut along a crystal diagonal plane. Finally, $\theta=90°$ corresponds to $[\bar{1}2\bar{1}0]$.

TABLE I. Material parameters. Data for different materials are taken from references indicated in the first row unless otherwise specified. As in Ref. 35 we assume $e_{15}=e_{31}$ (except for ZnO) and $\epsilon_{xx}=\epsilon_{zz}$ for MgO due to lack of data. We use linear interpolation to obtain parameters for nonbinary compounds.

	GaN[a]	AlN[a]	ZnO[b]	MgO[c]
e_{33} (C/m^2)	0.73	0.97	1.32	1.64
e_{15} (C/m^2)	−0.49	−0.57	−0.48	−0.58
e_{31} (C/m^2)	−0.49	−0.57	−0.57	−0.58
$c_{11}^{\mathbf{E}}$ (GPa)	390	396	210	222
$c_{12}^{\mathbf{E}}$ (GPa)	145	137	121	90
$c_{13}^{\mathbf{E}}$ (GPa)	106	108	105	58
$c_{33}^{\mathbf{E}}$ (GPa)	398	373	211	109
$c_{44}^{\mathbf{E}}$ (GPa)	105	116	42	105
$\epsilon_{xx}^{\mathbf{S}}/\epsilon_0$	9.28	8.67	9.16	9.8[d]
$\epsilon_{zz}^{\mathbf{S}}/\epsilon_0$	10.01	8.57	12.64	9.8[d]
P_{sp} (C/m^2)	−0.029	−0.081	−0.022[c]	−0.068[d]
a (10^{-10} m)	3.189	3.112	3.20[c]	3.45
c (10^{-10} m)	5.185	4.982	5.15[c]	4.14

[a]Reference 35 (experiment).
[b]Reference 22 (not specified).
[c]Reference 36 (*ab initio* calculations).
[d]Reference 19 (*ab initio* calculations).

First we discuss the case where $x=1$, i.e., GaN/AlN/GaN. We see from Fig. 2(a) that the magnitude of the longitudinal strain $S_{zz}^{(2)}$ for a [0001] growth direction changes significantly between the two models in agreement with previous findings.[23] We also see that model differences become less significant when the growth direction changes away from

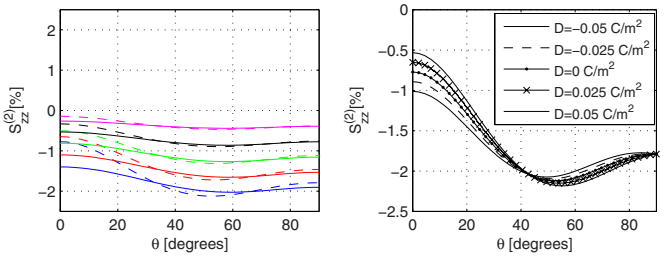

FIG. 2. (Color online) Longitudinal strain $S_{zz}^{(2)}$ in the middle layer for (a) GaN/$Ga_{1-x}Al_xN$/GaN with several x values and $D=0$ C/m^2. The colors blue, red, green, black, and magenta correspond to $x=1$, $x=0.8$, $x=0.6$, $x=0.4$, and $x=0.2$, respectively (with blue being the bottom and magenta the uppermost graphs). Solid (dashed) lines correspond to the semicoupled (fully coupled) model and for (b) several applied electric displacement fields D, using the fully coupled model for $x=1$.

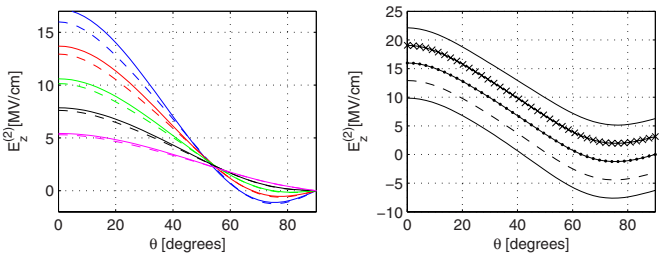

FIG. 3. (Color online) Electric field component $E_z^{(2)}$ in the middle layer for (a) $GaN/Ga_{1-x}Al_xN/GaN$ with several x values and $D=0$ C/m^2. The colors blue, red, green, black, and magenta correspond to $x=1$, $x=0.8$, $x=0.6$, $x=0.4$, and $x=0.2$, respectively (with magenta being the bottom and blue the uppermost graphs at $\theta=0$). Solid (dashed) lines correspond to the semicoupled (fully coupled) model and for (b) several applied electric displacement fields D, using the fully coupled model [same legend as Fig. 2(b)].

[0001]. Nevertheless, the angle of maximum longitudinal strain for magnitude is changed by almost 10° for $x=1$ when $D=0$ and similar for other D values (not shown). Also, the fully coupled model predicts a larger change in longitudinal strain as we change the growth direction. While for $x=1$ the semicoupled model predicts a range from −1.4% to −2% (the maximum-strain magnitude is about 1.5 times as large as for the [0001] growth direction), the fully coupled model predicts a range from −0.8% to −2.1% and the maximum-strain magnitude is almost three times as large as for the [0001] growth direction! Further, as we see in Fig. 3(a), the electric field for $x=1$ in the quantum well reverses direction in the interval from approximately $\theta=65°$ to $\theta=90°$ being zero close to $\theta=65°$ for $D=0$. Furthermore we see in Fig. 3(b) that the location of the electric field zero point changes for different values of D with no zero point for too high or too low values of D. Another interesting observation is the strain dependence on the applied electric displacement field D [Fig. 2(b)]. In actual fact, there is a growth direction for which the longitudinal strain is independent of the applied electric potential, since it is independent of the electric displacement D [refer to Fig. 2(b) for $\theta\approx 43°$].

We next discuss the longitudinal strain in $GaN/Ga_{1-x}Al_xN/GaN$ structures with the Al content varying [Fig. 2(a)]. As the content of Al increases in the central layer in the range 0.2–1, $S_{zz}^{(2)}$ values decrease from −0.1% when $x=0$, nearly independent of the second-rotation angle θ, to approximately −0.8% at $\theta=0$ and −1.9% at $\theta=90°$ when $x=1$. There is an increasing deviation between fully coupled and semicoupled model results as x increases especially at small θ angles. The large discrepancy is in agreement with data in Table I of Ref. 23 (row 1) corresponding to $\theta=0$ where the difference between fully coupled and semicoupled $S_{zz}^{(2)}$ values amounts to approximately 36%. It should also be mentioned that the difference between fully coupled and semicoupled models for the strain component $S_{zz}^{(2)}$ becomes less significant with increasing angle for all x values.

The electric field for $GaN/Ga_{1-x}Al_xN/GaN$ structures in the x range: 0.2–1 is shown in Fig. 3(a). Similar to the results for the strain component $S_{zz}^{(2)}$, the electric field is largest at an angle $\theta=0$ for all x values. Further, it is found that the electric field increases from nearly 5 MV/cm to 17 MV/cm in the

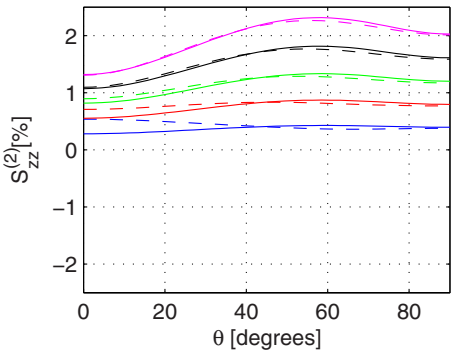

FIG. 4. (Color online) Longitudinal strain $S_{zz}^{(2)}$ for $AlN/Ga_xAl_{1-x}N/AlN$ with several x values and $D=0$ C/m^2. The colors blue, red, green, black, and magenta correspond to $x=0.2$, $x=0.4$, $x=0.6$, $x=0.8$, and $x=1$, respectively (with blue being the bottom and magenta the uppermost graphs). Solid (dashed) lines correspond to the semicoupled (fully coupled) model.

fully coupled case at $\theta=0$ as x increases from 0.2 to 1, and, as mentioned above, becomes zero for all x values at an angle $\theta=90°$. Notice that a second angle for which the electric field becomes zero is found at angles: $\theta=77°$, $\theta=68°$, and $\theta=62°$ when $x=0.6$, $x=0.8$, and $x=1$, respectively. Calculating the electric and deformation energy densities according to

$$W_{\text{elec}} = \frac{1}{2}\mathbf{E}^T \cdot \boldsymbol{\epsilon}^{\mathbf{S}} \cdot \mathbf{E} + \frac{1}{2}\mathbf{e} \cdot \mathbf{E}^T \cdot \mathbf{S}, \tag{15}$$

$$W_{\text{deform}} = \frac{1}{2}\mathbf{S}^T \cdot \mathbf{c}^{\mathbf{E}} \cdot \mathbf{S} - \frac{1}{2}\mathbf{e} \cdot \mathbf{E}^T \cdot \mathbf{S} \tag{16}$$

yields a total $(W_{\text{elec}}+W_{\text{deform}})$ energy density of 3.8×10^8 J/m^3 with the deformation energy density alone being 3.1×10^8 J/m^3 distributed uniformly in the middle layer with growth direction [0001]. Comparing to results given in Fig. 8a of Ref. 5 we obtain good agreement as they find an energy density of $\sim 2.9\times10^8$ J/m^3 in Ref. 5 disregarding electric effects.

B. $AlN/Ga_xAl_{1-x}N/AlN$ quantum well

Next, we discuss the influence on electromechanical fields by varying the content of Ga in $AlN/Ga_xAl_{1-x}N/AlN$ quantum well structures. In Fig. 4, $S_{zz}^{(2)}$ strain data are shown for $AlN/Ga_xAl_{1-x}N/AlN$ quantum well structures in the cases $x=0.2, 0.4, 0.6, 0.8, 1$, respectively. Evidently, as the amount of Ga in the middle quantum well layer increases, $S_{zz}^{(2)}$ values increase from approximately 0.6% to 1.3% at an angle $\theta=0$ in the fully coupled case. While the dependence on θ is weak for $x=0.2$, the second-rotation angle dependence becomes increasingly significant as x increases, and when $x=1$, $S_{zz}^{(2)}$ is nearly 2.2% for $\theta=60°$ compared to 1.3% at $\theta=0$. Since strain values are driven by the lattice mismatch between GaN and AlN this general tendency with x is not surprising. In contrast, our computations indicate that the deviations between fully coupled and semicoupled results decrease with increasing x due to a nonvanishing spontaneous polarization

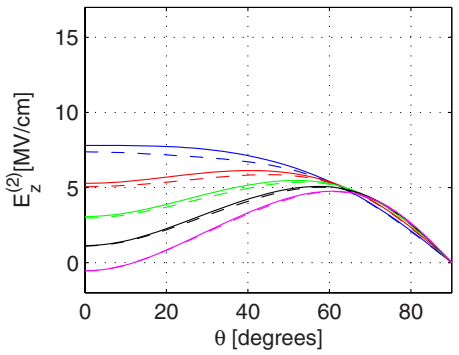

FIG. 5. (Color online) Electric field $E_z^{(2)}$ for $AlN/Ga_xAl_{1-x}N/AlN$ with several x values and $D=0$ C/m^2. The colors blue, red, green, black, and magenta correspond to $x=0.2$, $x=0.4$, $x=0.6$, $x=0.8$, and $x=1$, respectively (with magenta being the bottom and blue the uppermost graphs at $\theta=0$). Solid (dashed) lines correspond to the semicoupled (fully coupled) model.

while fixing $D=0$ everywhere. This result follows directly from Eq. (13) with $a_{mis}=0$. We also note that the negligible difference between fully coupled and semicoupled results for the AlN/GaN/AlN structure agrees with earlier conclusions.[23] In actual fact, it was shown in Table I of Ref. 23 (row 4), that the sum of the two strain contributions arising from spontaneous polarization and piezoelectric effects amounts to only −0.06% in GaN films grown on a AlN substrate!

In Fig. 5, electric field data are plotted vs second-rotation angle θ for the same set of x values as in Fig. 4. The electric field is strongly dependent on the rotation angle θ and changes from 8 MV/cm to 0 as θ changes from 0° to 90° in the case with $x=0.2$. The absolute maximum electric field value is obtained for an angle $\theta=0$ when $x=0.2$, however, for $x\geq 0.4$, the electric field maximum (close to 5 MV/cm) is obtained near $\theta=60°$. For all Ga content values, the electric field vanishes when the rotation angle is 90°. This is due to the fact that the z component of the spontaneous polarization vanishes and $(e\cdot S)_z=e_{15}S_4=0$ when $\theta=90°$ since $D=0$ everywhere. We see that, for $x=1$ there also is an electric field zero point apart from $[\bar{1}2\bar{1}0]$ in the well region. We observe that the diminishing difference between fully coupled and semicoupled model results with increasing x, found in the case of $S_{zz}^{(2)}$, appears also for the electric field.

C. ZnO/Mg_xZn_{1-x}O/ZnO antiwell

Apart from investigating nitride-based antiwell structures (GaN/AlN/GaN), which show the same general behavior in terms of quality of the semicoupled model vs a fully coupled model as well as reversing of the electric field with varying orientation, we also analyzed a $ZnO/Mg_{0.3}Zn_{0.7}/ZnO$ antiwell heterostructure. Results for this structure are shown in Figs. 6, 7(b), and 8(b). As seen in Fig. 7(b), the quality of the semicoupled model for $S_{zz}^{(2)}$ is in the same order of magnitude as for the GaN/AlN/GaN structure considered above, however, it is slightly better. In contrast to the GaN/AlN/GaN structure we see in Fig. 6(a) that the quality of the semicoupled model becomes inaccurate for the shear-strain component S_{yz} in the range: $45°<\theta<80°$, a region where the shear strain can be even larger than the longitudinal strain. A change in sign occurs for the shear strain in this region and calculations for binary MgO in the quantum well region show that this discrepancy becomes even larger when the Mg content is increased. Even though binary MgO is not in wurtzite phase anymore (rocksalt), molecular beam epitaxy growth of wurtzite $Mg_xZn_{1-x}O$ up to $x=0.5$ has been reported.[6] It can be seen in Fig. 6(b) that a growth direction exists where the shear strain does not depend on the applied electric displacement field D. Hence, it is independent of the applied electric potential across the heterostructure (note, however, that this does not occur at the same growth direction as for the longitudinal strain component). Another interesting observation is the electric field behavior in the quantum well region [Figs. 8(b) and 8(d)] where the electric field reverses direction twice. Thus, there are two growth directions apart from 90° for which the electric field in the middle region is zero.

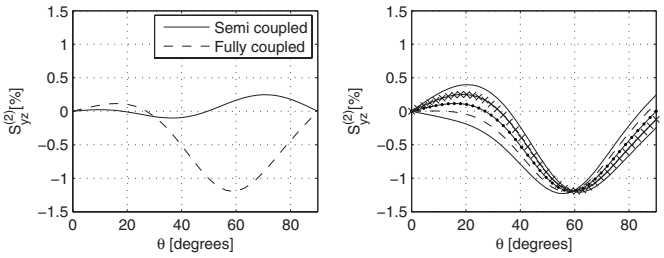

FIG. 6. Shear-strain component $S_{yz}^{(2)}$ in the middle layer ($ZnO/Mg_{0.3}Zn_{0.7}O/ZnO$ heterostructure) for (a) the fully coupled and semicoupled models corresponding to $D=0$ C/m^2 and for (b) several applied electric displacement fields D using the fully coupled model [same legend as in Fig. 2(b)].

We also examined the influence of a varying Mg content in $ZnO/Mg_xZn_{1-x}O/ZnO$ structures. The longitudinal strain for $ZnO/Mg_xZn_{1-x}O/ZnO$ structures in the cases $x=0.1$, x

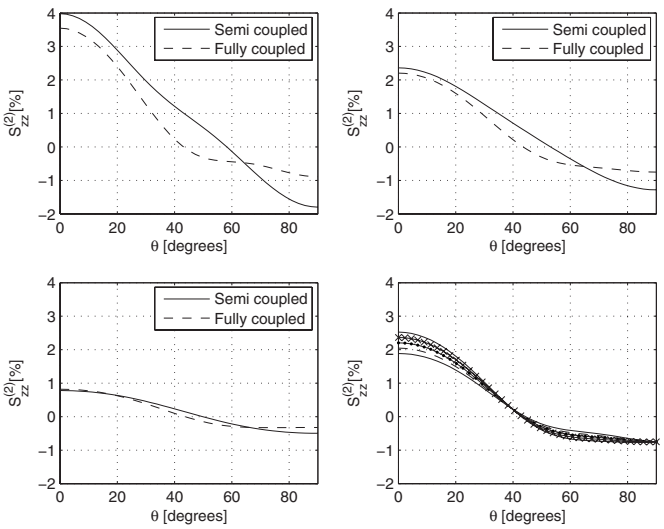

FIG. 7. Longitudinal strain $S_{zz}^{(2)}$ for $ZnO/Mg_xZn_{1-x}O/ZnO$ with $D=0$ C/m^2 and (a) $x=0.5$, (b) $x=0.3$, (c) $x=0.1$, and (d) $x=0.3$ for several applied electric displacement fields using the fully coupled model [same legend as in Fig. 2(b)].

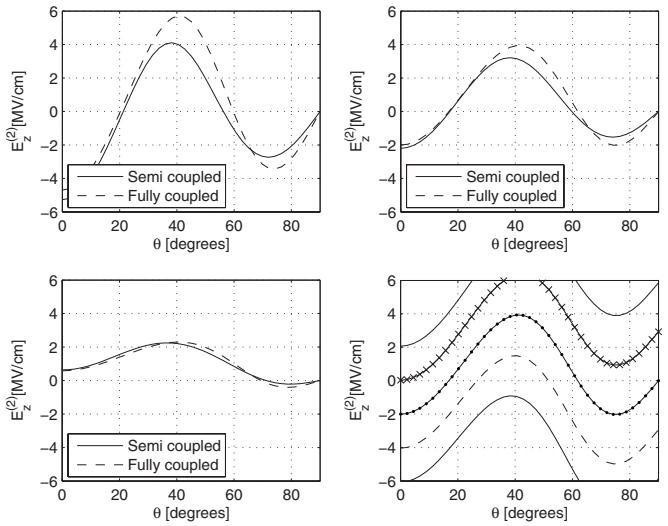

FIG. 8. Electric field $E_z^{(2)}$ for $ZnO/Mg_xZn_{1-x}O/ZnO$ with $D=0$ C/m^2 and (a) $x=0.5$, (b) $x=0.3$, (c) $x=0.1$, and (d) $x=0.3$ for several applied electric displacements D using the fully coupled model [same legend as in Fig. 2(b)].

$=0.3$, and $x=0.5$ is shown in Fig. 7. As expected, it is found that the strain $S_{zz}^{(2)}$ increases for increasing x with a maximum value of 3.5% at $x=0.5$ and $\theta=0°$. The strain depends strongly on the second-rotation angle θ even in cases with a smaller x. For $x=0.1$, we see that the strain decreases from 0.9% to −0.3% as θ goes from 0° to 90°. As for the $GaN/Ga_xAl_{1-x}N/GaN$, the accuracy of the semicoupled model for this structure decreases as x increases. This is due to the relatively high piezoelectric constants compared with the spontaneous polarization for the $Mg_xZn_{1-x}O$ layer.

Furthermore we discuss the electric field in the $Mg_xZn_{1-x}O$ layer as shown in Fig. 8. The electric field in this case is not having its maximum at $\theta=0°$. For example, the absolute maximum (5.5 MV/cm) is found at $\theta=40°$ when $x=0.5$. We also see that apart from $\theta=90°$ there are two second-rotation angle values θ where the electric field becomes zero if $x=0.5$ and $x=0.3$. For $x=0.5$ these angles are: $\theta=15°$ and $\theta=65°$. Further, for $x=0.3$ they are: $\theta=18°$ and $\theta=62°$. For $x=0.1$, there is only one angle (at $\theta=70°$) where the electric field vanishes apart from $\theta=90°$. Indeed, this shows that in order to obtain extra angles for a vanishing electric field the piezoelectric misfit contribution must be large compared to the spontaneous polarization contribution.

D. $Mg_xZn_{1-x}O/ZnO/Mg_xZn_{1-x}O$ quantum well

Finally we discuss the $Mg_xZn_{1-x}O/ZnO/Mg_xZn_{1-x}O$ quantum well structure. Results for this structure are shown in Figs. 9, 10(b), and 11(b). First we focus on the case $x=0.3$, as this seems to be the most commonly used alloy. As seen in Fig. 10(b), the quality of the semicoupled model for $S_{zz}^{(2)}$ is in the same order of magnitude as for the AlN/GaN/AlN structure considered above, however, it is slightly worse. However, for the shear-strain component, shown in Fig. 9(a), we see that the semicoupled model becomes inaccurate in regions where $45° < \theta < 80°$. In this region the

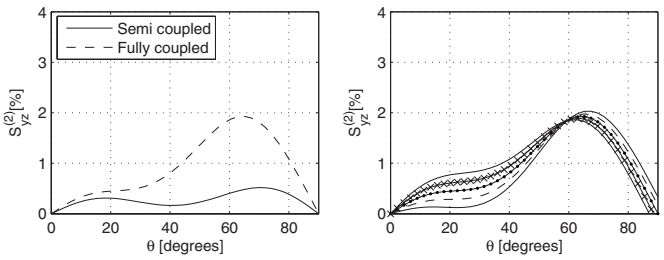

FIG. 9. Shear-strain component $S_{yz}^{(2)}$ in the quantum well layer ($Mg_{0.3}Zn_{0.7}O/ZnO/Mg_{0.3}Zn_{0.7}O$ heterostructure) for (a) the fully coupled and semicoupled models corresponding to $D=0$ C/m^2 and for (b) several applied electric displacement fields D using the fully coupled model [same legend as in Fig. 2(b)].

shear strain can be even larger than the longitudinal strain. It can be seen in Fig. 10(d) that as with the $ZnO/Mg_{0.3}Zn_{0.7}O/ZnO$ case a growth direction exists where the shear strain does not depend on the applied electric displacement field D, thus being independent of the applied electric potential across the heterostructure. In contrast to the electric field in the middle layer for the corresponding antiwell structure, the electric field in the quantum well layer as depicted in Fig. 11(b) does not change direction with change in growth direction at $D=0$. However, there is a local minimum at 40°, and as seen in Fig. 11(d), applying an appropriate electric displacement results in two zero crossings. Note that in this case, $\theta=90°$ does not correspond to a vanishing electric field anymore.

We also examined the influence of a varying Zn content in $Mg_xZn_{1-x}O/ZnO/Mg_xZn_{1-x}O$ structures. The longitudinal strain for $Mg_xZn_{1-x}O/ZnO/Mg_xZn_{1-x}O$ structures in the cases $x=0.1$, $x=0.3$, and $x=0.5$ is shown in Fig. 10. We see that the longitudinal strain increases for increasing value of x. The maximum (absolute) value is 3% and varies from −3% at $\theta=0°$ to more than 2% at $\theta=90°$. Even for small x, the strain varies from −0.6% to 0.4%.

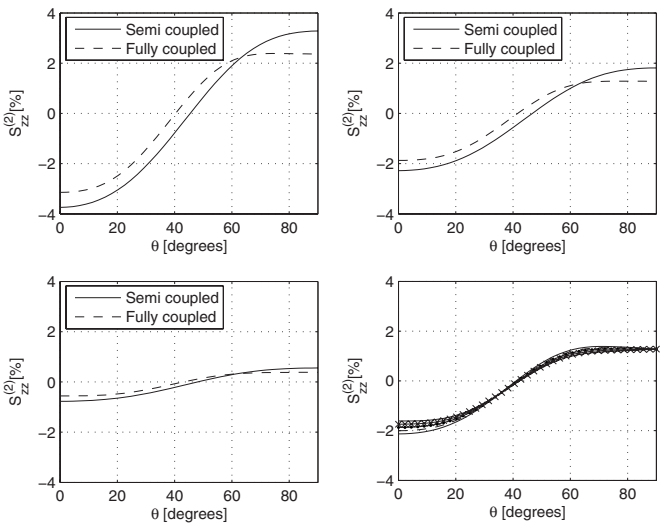

FIG. 10. Longitudinal strain $S_{zz}^{(2)}$ for $Mg_xZn_{1-x}O/ZnO/Mg_xZn_{1-x}O$ with $D=0$ C/m^2 and (a) $x=0.5$, (b) $x=0.3$, (c) $x=0.1$, and (d) $x=0.3$ for several applied electric displacement fields using the fully coupled model [same legend as in Fig. 2(b)].

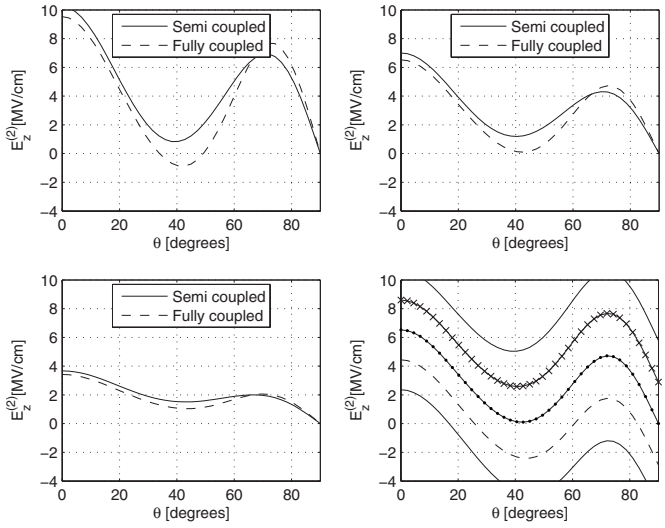

FIG. 11. Electric field $E_z^{(2)}$ for $Mg_xZn_{1-x}O/ZnO/Mg_xZn_{1-x}O$ with $D=0$ C/m^2 and (a) $x=0.5$, (b) $x=0.3$, (c) $x=0.1$, and (d) $x=0.3$ for several applied electric displacements D using the fully coupled model [same legend as in Fig. 2(b)].

In Fig. 11 we see that the electric field at $D=0$ does starts changing direction for higher Mg contents. At $x=0.5$ we observe that the electric field changes direction for θ ranging from 30° to 50° having two electric field zero points. This supports our statement above that the piezoelectric misfit contribution must be large compared to the spontaneous polarization contribution in order to obtain zeros in the electric field in the middle layer.

IV. CONCLUSION

We have presented and solved fully coupled electromechanical one-dimensional equations for a three-layer antiwell GaN/AlN/GaN and $ZnO/Mg_xZn_{1-x}O/ZnO$ structures and $AlN/Ga_xAl_{1-x}N/AlN$ and $ZnO/Mg_xZn_{1-x}O/ZnO$ quantum well heterostructures with arbitrary unit-cell orientation relative to the structure growth direction. The longitudinal strain component along the growth direction varies significantly with the growth direction and a maximum magnitude for a GaN/AlN/GaN structure is found at a growth direction of approximately 50° in contrast to the 60° predicted by the semicoupled model (for $D=0$). Also, we find that the electric field in the well layers of the AlN/GaN/AlN structure, crucial in the design of quantum-efficient LEDs,[15] has a zero crossing in the region between $[0001]$ and $[\bar{1}2\bar{1}0]$ apart from $[\bar{1}2\bar{1}0]$. For the $Mg_{0.3}Zn_{0.7}/ZnO/Mg_{0.3}Zn_{0.7}$ structure investigated, we find a local minimum at $\theta=40°$, where the electric field is very close to zero. Increasing the Mg content to 0.5, we find two zeros apart from $[\bar{1}2\bar{1}0]$. Furthermore, for all structures investigated, certain growth directions are obtained where the longitudinal strain does not depend on the applied electric displacement D while the electric field does. For the oxide structures, the accuracy of the semicoupled model is worse for the shear-strain component as compared to the longitudinal strain component. An important result is that for certain growth directions, the shear-strain component is significantly larger than the longitudinal strain making the semicoupled model inaccurate for ZnO/MgZnO/ZnO and MgZnO/ZnO/MgZnO structures. Here, we also find a growth direction where the shear-strain component is independent of the applied electric potential.

The present study emphasizes the need to use a fully coupled model in calculating strain distributions for different growth directions. Further, we see that the electric field in GaN/AlN/GaN antiwell structures shows a zero crossing when changing the growth direction. For $ZnO/Mg_xZn_{1-x}O/ZnO$ and $Mg_xZn_{1-x}O/ZnO/Mg_xZn_{1-x}O$ structures we even find up to two zero crossings apart from $[\bar{1}2\bar{1}0]$ of the electric field as a function of the growth orientation angle.

*duggen@mci.sdu.dk

[1] S. Nakamura, T. Mukai, and M. Senoh, Appl. Phys. Lett. **64**, 1687 (1994).
[2] M. Kneissl, D. W. Treat, M. Teepe, N. Miyashita, and N. M. Johnson, Appl. Phys. Lett. **82**, 4441 (2003).
[3] H. Yoshida, Y. Yamashita, M. Kuwabara, and H. Kan, Nat. Photonics **2**, 551 (2008).
[4] H. Yoshida, Y. Yamashita, M. Kuwabara, and H. Kan, Appl. Phys. Lett. **93**, 241106 (2008).
[5] A. Bykhovski, B. Gelmont, and M. Schur, J. Appl. Phys. **78**, 3691 (1995).
[6] S. Fujita, T. Takagi, H. Tanaka, and S. Fujita, Phys. Status Solidi B **241**, 599 (2004).
[7] W. J. Fan, J. B. Xia, P. A. Agus, S. T. Tan, S. F. Yu, and X. W. Sun, J. Appl. Phys. **99**, 013702 (2006).
[8] S.-H. Park and D. Ahn, Appl. Phys. Lett. **87**, 253509 (2005).
[9] G. Coli and K. K. Bajaj, Appl. Phys. Lett. **78**, 2861 (2001).
[10] W. J. Fan, A. P. Abiyasa, S. T. Tan, S. F. Yu, X. W. Sun, J. B. Xia, Y. C. Yeo, M. F. Li, and T. C. Chong, J. Cryst. Growth **287**, 28 (2006).
[11] S. Sasa, M. Ozaki, K. Koike, M. Yano, and M. Inoue, Appl. Phys. Lett. **89**, 053502 (2006).
[12] K. Koike, I. Nakashima, K. Hashimoto, S. Sasa, M. Inoue, and M. Yano, Appl. Phys. Lett. **87**, 112106 (2005).
[13] S.-H. Park and S.-L. Chuang, Appl. Phys. Lett. **72**, 3103 (1998).
[14] S.-H. Park and S.-L. Chuang, Phys. Rev. B **59**, 4725 (1999).
[15] P. Waltereit, O. Brandt, A. Trampert, H. T. Grahn, J. Menniger, M. Ramsteiner, M. Reiche, and K. H. Ploog, Nature (London) **406**, 865 (2000).
[16] A. Bykhovski, B. Gelmont, and M. Shur, Appl. Phys. Lett. **63**, 2243 (1993).
[17] S. Khatsevich and D. H. Rich, J. Phys.: Condens. Matter **20**, 215223 (2008).
[18] T. Ohtoshi, A. Niwa, and T. Kuroda, J. Appl. Phys. **82**, 1518 (1997).
[19] S.-H. Park and D. Ahn, Opt. Quantum Electron. **38**, 935 (2007).

[20] S.-H. Park and S.-L. Chuang, J. Appl. Phys. **87**, 353 (2000).
[21] M. Willatzen, IEEE Trans. Ultrason. Ferroelectr. Freq. Control **48**, 100 (2001).
[22] B. Auld, *Acoustic Fields and Waves in Solids*, 2nd ed. (Krieger, Malabar, Florida, 1990), Vol. I.
[23] M. Willatzen, B. Lassen, L. C. Lew Yan Voon, and R. V. N. Melnik, J. Appl. Phys. **100**, 024302 (2006).
[24] L. Duggen, M. Willatzen, and B. Lassen, Phys. Rev. B **78**, 205323 (2008).
[25] L. D. Landau and E. M. Lifshitz, *Theory of Elasticity*, Course of Theoretical Physics (Butterworth Heinemann, Oxford, UK, 1986).
[26] C.-N. Chen, S.-H. Chang, M.-L. Hung, J.-C. Chiang, I. Lo, W.-T. Wang, M.-H. Gau, H.-F. Kao, and M.-E. Lee, J. Appl. Phys. **101**, 043104 (2007).
[27] J. Singh, *Electronic and Optoelectronic Properties of Semiconductor Structures* (Cambridge University Press, Cambridge, 2003).
[28] P. N. Keating, Phys. Rev. **145**, 637 (1966).
[29] D. Barettin, S. Madsen, B. Lassen, and M. Willatzen, Proceedings of ICPS 2010, Seoul, Korea, 2010 (in press).
[30] L. Guy, S. Muensit, and E. M. Goldys, Appl. Phys. Lett. **75**, 3641 (1999).
[31] R. E. Newnham, V. Sundar, R. Yimnirun, J. Su, and Q. M. Zhang, J. Phys. Chem. B **101**, 10141 (1997).
[32] M. Willatzen and L. C. L. Y. Voon, J. Phys.: Condens. Matter **19**, 506202 (2007).
[33] I. Kornev, M. Willatzen, B. Lassen, and L. L. Y. Voon, AIP Conf. Proc. No. 1199 (AIP, New York, 2010), p. 71.
[34] M. Willatzen, B. Lassen, and L. C. L. Y. Voon, J. Appl. Phys. **100**, 124309 (2006).
[35] V. A. Fonoberov and A. A. Balandin, J. Appl. Phys. **94**, 7178 (2003).
[36] P. Gopal and N. A. Spaldin, J. Electron. Mater. **35**, 538 (2006).